A Wavy Two-Dimensional Conjugated Metal–organic Framework with Metallic Charge Transport

Jianjun Zhang[1,‡], Guojun Zhou[2,‡], Hio-Ieng Un[3,‡], Fulu Zheng[4,‡], Kamil Jastrzembski[1,‡], Mingchao Wang[1], Quanquan Guo[1,5], David Mücke[6], Haoyuan Qi[6], Yang Lu[1,5], Zhiyong Wang[1,5,*] Yan Liang[4], Markus Löffler[7], Ute Kaiser[6], Thomas Frauenheim[8,9,10], Aurelio Mateo-Alonso[11,12], Zhehao Huang[2,*], Henning Sirringhaus[3,*], Xinliang Feng[1,5,*], Renhao Dong[1,13*]

[1]Center for Advancing Electronics Dresden (cfaed) and Faculty of Chemistry and Food Chemistry, Technische Universität Dresden, Dresden 01062, Germany

[2]Department of Materials and Environmental Chemistry, Stockholm University, Stockholm SE-106 91, Sweden

[3] Optoelectronics Group, Department of Physics, Cavendish Laboratory, University of Cambridge, Cambridge CB3 0HE, United Kingdom

[4]Bremen Center for Computational Materials Science, University of Bremen, Bremen 28359, Germany

[5]Max Planck Institute for Microstructure Physics, Weinberg 2, Halle (Saale) 06120, Germany

[6]Central Facility for Electron Microscopy, Electron Microscopy of Materials Science Central, Facility for Electron Microscopy, Ulm University, Ulm 89081, Germany

[7]Dresden Center for Nanoanalysis (DCN), Center for Advancing Electronics Dresden (Cfaed), Technische Universität Dresden, Dresden 01069, Germany

[8]Constructor University, Campus Ring 1, Bremen 28759, Germany

[9]Beijing Computational Science Research Center, Beijing 100193, China

[10]Shenzhen JL Computational Science and Applied Research Institute, Shenzhen 518109, China

[11]POLYMAT, University of the Basque Country UPV/EHU, Avenida de Tolosa 72, Donostia-San Sebastian 20018, Spain

[12]Ikerbasque, Basque Foundation for Science, Bilbao 48011, Spain

[13]Key Laboratory of Colloid and Interface Chemistry of the Ministry of Education, School of Chemistry and Chemical Engineering, Shandong University, Jinan 250100, China

ABSTRACT: Two-dimensional conjugated metal-organic frameworks (2D c-MOFs) have emerged as a new class of crystalline layered conducting materials that hold significant promise for applications in electronics and spintronics. However, current 2D c-MOFs are mainly made from organic planar ligands, whereas layered 2D c-MOFs constructed by curved or twisted ligands featuring novel orbital structures and electronic states remain less developed. Herein, we report a Cu-catecholate wavy 2D c-MOF ($Cu_3(HFcHBC)_2$) based on fluorinated core-twisted contorted hexahydroxy-hexa-cata-hexabenzocoronene (HFcHBC) ligand. We show that the resulting film is composed of rod-like single crystals with length up to ~ 4 μm. The crystal structure is resolved by high-resolution transmission electron microscopy (HRTEM) and continuous rotation electron diffraction (cRED), indicating a wavy honeycomb lattice with an AA eclipsed stacking. $Cu_3(HFcHBC)_2$ is predicted to be metallic based on theoretical calculation, while the crystalline film sample with numerous grain boundaries exhibits apparently semiconducting behavior at the macroscopic scale, characterized by obvious thermally-activated conductivity. Temperature-dependent electrical conductivity measurements on the isolated single crystal devices demonstrate indeed the metallic nature of $Cu_3(HFcHBC)_2$, with a very weak thermally-activated transport behavior and a room temperature conductivity of 5.2 S cm^{-1}. Furthermore, the 2D c-MOFs can be utilized as potential electrode materials for energy storage, which display decent capacity (163.3 F g^{-1}) and excellent cyclability in aqueous 5M LiCl electrolyte. Our work demonstrates that wavy 2D c-MOFs using contorted ligands are capable of intrinsic metallic transport, marking the emergence of new conductive MOFs for electronic and energy applications.

INTRODUCTION

Two-dimensional conjugated metal-organic frameworks (2D c-MOFs) are an emerging class of crystalline electronic and spintronic materials.[1] These materials are characterized by a typical van der Waals layer-stacked structure that facilitates efficient charge transport in both in-plane and out-of-plane directions, resulting in unique physical properties such as excellent electrical conductivity, tailorable band gaps, and high charge carrier mobility.[2-4] Such features render 2D c-MOFs potential candidates for applications in opto-electronics[5-7] and thermoelectrics,[8-9] energy storage and conversion.[10-11] Typically, 2D c-MOFs are constructed by the periodic connection of π-conjugated organic ligands via square-planar MX_4 linkages (M=metal ion, X= O, NH, S),[12-14] resulting in a diverse range of topological networks such as hexagonal, honeycomb, kagome and square lattices.[1] Nonetheless, there are only dozens of 2D c-MOFs available, which are exclusively derived from planar conjugated aromatic hydrocarbons including phthalocyanine,[15-17] coronene,[18] triphenylene,[12-13, 19] and benzene.[20-22]

Non-planar polycyclic aromatic hydrocarbons (PAHs) such as corannulenes,[23] circulenes,[24] sumanene,[25] and contorted hexa-cata-hexabenzocoronene (cHBC)[26-27] possess a contorted topology that differs from their planar counterparts, enabling manipulation of orbital structures and electronic states across concave and convex faces. The asymmetric charge-distribution on the concave and convex faces can act as donors and acceptors, thereby promoting electronic communication within the supramolecular assemblies, and resulting in unique physical properties, such

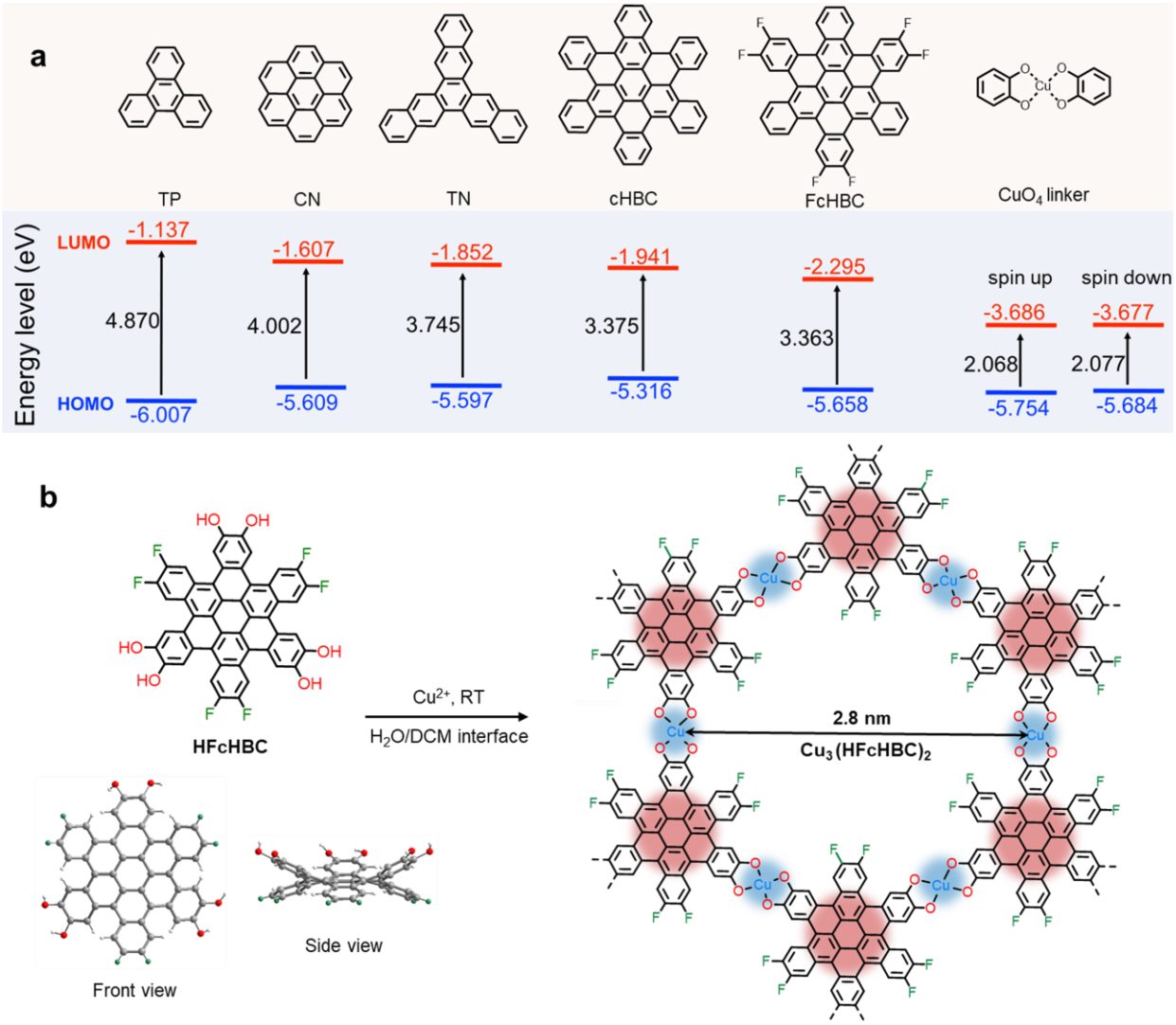

Figure 1. Design and synthesis of $Cu_3(HFcHBC)_2$. (a) Chemical structure and energies of highest occupied molecular orbital (HOMO) and lowest unoccupied molecular orbital (LUMO) of the TP, CN, TN, cHBC, FcHBC ligand core and CuO_4 linker. (b) Chemical structure of HFcHBC with the front view and side view and the resulted $Cu_3(HFcHBC)_2$ 2D c-MOF structure. C, O, F and H atoms are shown in grey, red, green and white, respectively.

as intramolecular charge transfer,[28] thermally activated delayed fluorescence,[29] and long-lived charge-separation states.[30] Furthermore, the concave-convex self-complementarity of non-planar building blocks can facilitate the formation of highly ordered stacking column structures, thereby offering a promising avenue for the synthesis of single crystals. Very recently, cHBC nodes have been introduced in covalent organic frameworks[31-33] and 2D c-MOFs[34], which have given rise to unprecedented wavy 2D structures that deviate from the standard graphitic geometries. Despite recent progress in the synthesis of these unique wavy structures, the well-resolved single crystal structures and the intrinsic charge transport properties (semiconductor or metal) of the wavy 2D c-MOFs based on non-planar PAH ligands have remained elusive.

Here, we synthesized a novel wavy 2D c-MOF (named as $Cu_3(HFcHBC)_2$) film at a water/dichloromethane (DCM) interface based on the fluorinated core-twisted cHBC ligand, i.e., 2,3,10,11,18,19-hexafluoro-6,7,14,15,22,23-hexahydroxy cHBC (abbreviated as HFcHBC). The fluorination of cHBC leads to higher reversibility of the metal–ligand bond compared to the non-fluorinated cHBC, which contributes to the formation of rod-like single crystals with lengths up to ~4.0 μm. Continuous rotation electron diffraction (cRED) and high-resolution transmission electron microscopy (HRTEM) measurements demonstrate a wavy 2D honeycomb network with AA eclipsed stacking at the atomic level. Density functional theory (DFT) calculations suggest the metallic behavior of $Cu_3(HFcHBC)_2$, with the conduction band crossing the Fermi level in both *Γ-K* and *Γ-A* directions, indicating the efficient charge transport in both in-plane and out-of-plane directions. The temperature-dependent electrical conductivity measurement using the van der Pauw structure shows a semiconducting behavior of $Cu_3(HFcHBC)_2$ film, due to the thermally activated intergrain hopping dominates the conductivity. Notably, the temperature-dependent conductivity of the four-probe single crystal devices demonstrate the intrinsic metallic nature, with a room temperature conductivity of 5.2 S cm^{-1}. This work reports a metallic wavy 2D c-MOF based on fluorinated non-planar ligands, provides an effective ligand design strategy for the synthesis of 2D c-MOF single crystals, and highlights the potential of conductive MOFs for electronics and energy.

RESULTS AND DISCUSSION

In principle, the electronic structures of the ligands play a crucial role in determining the crystallinity of 2D c-MOFs and their charge transport properties. In light of this, we first performed DFT calculations to evaluate the design of the PAH ligand cores for 2D c-MOFs. As shown in Figures 1a and S1, the results indicate that the non-planar cHBC leads to a decreased electron density and a lower lowest unoccupied molecular orbital (LUMO) energy of -1.941 eV compared to the planar triphenylene (TP, LUMO: -1.137 eV), coronene (CN, LUMO: -1.607 eV) and trinaphthylene (TN, LUMO: -1.857 eV). To further optimize the electronic structure of the ligand, fluorinated cHBC (FcHBC) was further investigated, since fluorination has been established as a strategy for lowering the LUMO and highest occupied molecular orbital (HOMO) energy levels for improved electron transport in organic semiconductors.[35] The FcHBC core exhibits a notable down-shifted LUMO (-2.295 eV) compared to the parent cHBC (-1.941 eV). The electron-withdrawing F groups lead to the downshifted energy level, which can increase the acidity of the catechol groups in HFcHBC when compared to the reported 2,3,10,11,18,19-hexahydroxy cHBC (abbreviated as HHcHBC, Figures S1 and S2).[31, 34] The increased acidity promotes a significantly more reversible coordination reaction between the HFcHBC ligand and Cu node. As a result, the potential disorder of the metal-ligand bonds can be effectively corrected, thereby producing 2D c-MOF with high in-plane crystallinity.[36] Besides, the HFcHBC ligand adopts a C_{3v} symmetry, the concave and convex π-surfaces are beneficial for the long-range ordered π-stacking, resulting in efficient interlayer electronic coupling (Figure 1a).[31, 37] Moreover, the HFcHBC ligand core displayed matched energy-level alignment with the CuO_4 linkage (Figure 1a), which is favorable for efficient intralayer charge transport.[4] Therefore, on the one hand, the HFcHBC ligand is expected to achieve high crystallinity in both in-plane and out-of-plane directions during 2D c-MOF synthesis. On the other hand, the optimized energy-level alignment and interlayer electronic coupling promote favorable charge transport within the 2D c-MOF. Guided by the DFT calculations of the energy levels, we synthesized the HFcHBC ligand for the construction of wavy 2D c-MOF (Figure 1b).

The synthesis of HFcHBC ligand involved three steps that started with the Suzuki cross-coupling of 1,3,5-tri(bromomethyl)-benzene and 3,4-dimethoxyphenyl boronic acid, followed by three-fold cyclization reaction of the resulting product with 3,4-difluorobenzaldehydeary into the polycyclic aromatic architectures. Further deprotection with BBr_3 was then carried out to yield hydroxyl groups (Scheme S1, Figure S3 – S5). Next, we utilized a liquid-liquid interfacial synthesis method to construct the 2D c-MOF films (Figure S6).[38] In a typical synthetic procedure, a freshly prepared HFcHBC solution in dimethylformamide (DMF, 700 μl, 1 mg ml^{-1}) was slowly dropped onto dichloromethane (DCM, 20 ml) in a beaker (60 ml, diameter = 6 cm), and then the deionized water (10 ml) was added to form the water/ DCM interface. Afterward, an aqueous solution of copper (II) acetate (10 ml, 2 mg ml^{-1}) was injected into the water phase to initiate the coordination polymerization.

The resulting biphasic mixture was left undisturbed at room temperature for 3 h. A spontaneous reaction at the water/ DCM interface affords a continuous $Cu_3(HFcHBC)_2$ film with a lateral area of ~28 cm^2 (Figure S7), which could be transferred horizontally onto different substrates for

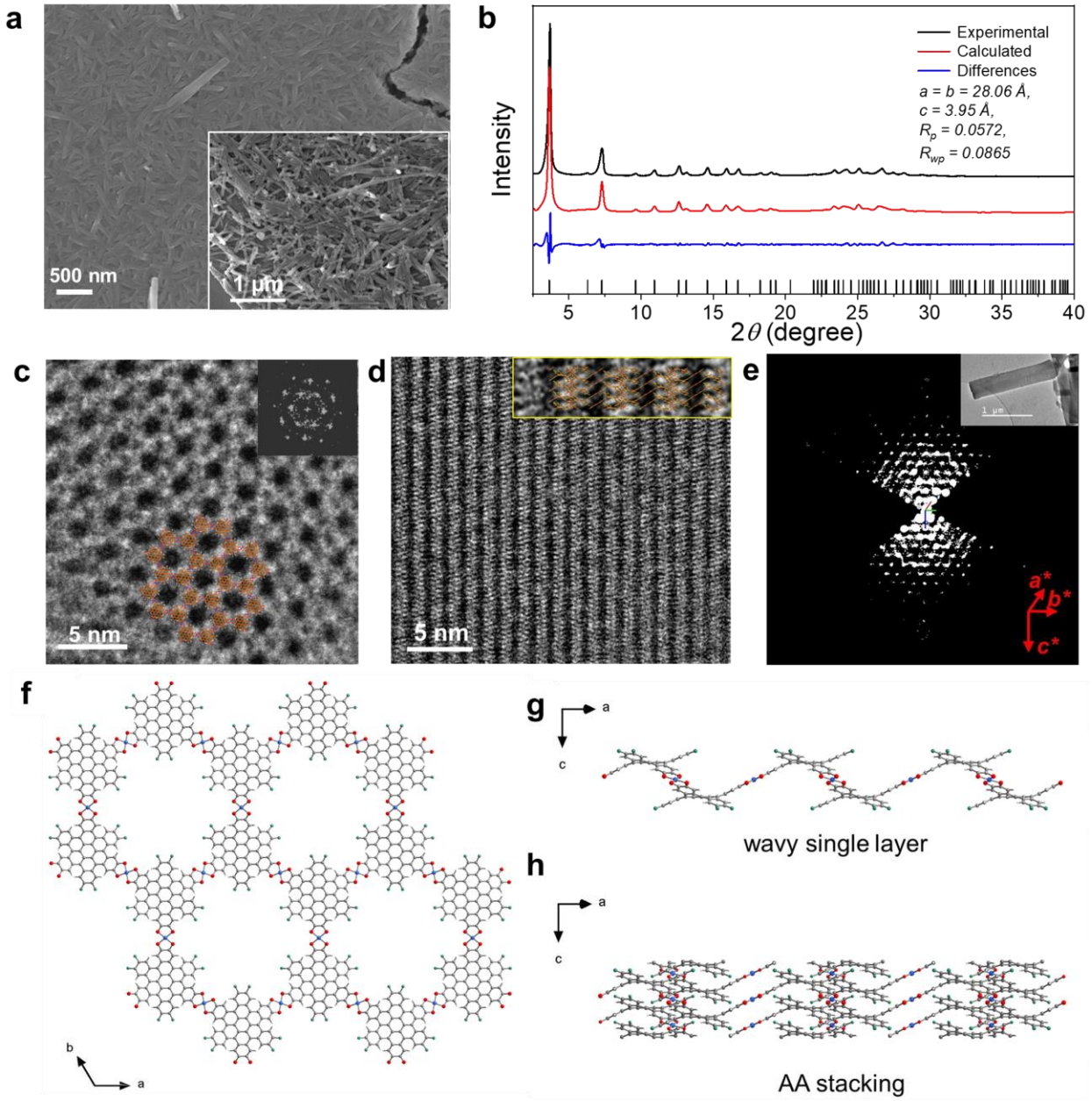

Figure 2. **Structural model of $Cu_3(HFcHBC)_2$ derived from PXRD, HRTEM and cRED.** (a) SEM image of $Cu_3(HFcHBC)_2$ film facing the water. Inset: film facing the DCM. (b) Overlay of the experimental PXRD pattern and Pawley fitting plots of $Cu_3(HFcHBC)_2$. HRTEM image of the $Cu_3(HFcHBC)_2$ film along (c) [001] direction, top inset: corresponding FFT image and (d) [110] direction, top inset: enlarged HRTEM image overlaid with structure mode. (e) Reconstructed three-dimensional reciprocal lattice based on cRED of a $Cu_3(HFcHBC)_2$ rod single crystal (Inset: $Cu_3(HFcHBC)_2$ single crystal on the Cu grid). (f, g, h) A portion of the $Cu_3(HFcHBC)_2$ crystal structure: projection view along the c-axis (f) and the wavy single-layer structure (g) and the AA stacking behavior (h). C, O, Cu, F and H atoms are shown in grey, red, blue, green and white, respectively.

morphological and structural characterizations. Optical microscopy (OM) image presents a continuous feature of $Cu_3(HFcHBC)_2$ film on the Si/SiO_2 substrate (Figure S7). Scanning electron microscopy (SEM) (Figure 2a) and atomic force microscopy (AFM) (Figure S8) images indicate that the resulting films facing the water are composed of dense rod-like crystals. In comparison, the films facing the DCM comprise of loosed-packed rod-like crystals, with lengths varying from 500 nm to 4 μm. Fourier-transform infrared (FT-IR) spectroscopy presents the absence of the -OH stretching vibration (~3200 cm^{-1}) from HFcHBC, demonstrating the successful coordination between Cu ion and HFcHBC (Figure S9). X-ray photoelectron spectros-

copy (XPS) and the SEM-energy dispersed X-ray spectroscopy mapping (SEM-EDS) show the distribution of Cu, F, O, and C elements in the $Cu_3(HFcHBC)_2$ sample (Figures S10 and S12). The high-resolution X-ray photoelectron spectroscopy (XPS) of Cu $2p_{3/2}$ displayed an asymmetric peak, which can be deconvoluted into two dominated peaks at 934.6 eV and 932.7 eV, respectively (Figure S10). These peaks correspond to the +2 and +1 oxidation states of Cu, respectively. The deconvolution of the Cu *2p* region indicated a ratio of 85% Cu(II) and 15% Cu(I). The absence of charge balancing counterions suggests that the charge variation from Cu(II) to Cu(I) is compensated by redox-active HFcHBC ligands (Figures S10 and S11).[39] The X-ray absorption near-edge structure (XANES) and extended X-ray absorption fine-structure (EXAFS) spectra of $Cu_3(HFcHBC)_2$ were collected to investigate the valency state of Cu and its coordination environment (Figure S13). The edge energy of $Cu_3(HFcHBC)_2$ is ~8982 eV, and it exhibits strikingly similar white line peaks to those of CuO, implying that the dominant valency state of Cu in $Cu_3(HFcHBC)_2$ is +2. By fitting the Cu K-edge EXAFS spectrum of $Cu_3(HFcHBC)_2$, we derived an average coordination number of 3.2 for Cu with Cu-O bond length of 1.94 Å (Table S2). The X-ray absorption measurements combined with single crystal analysis demonstrate the presence of the planar CuO_4 complex in the $Cu_3(HFcHBC)_2$. $Cu_3(HFcHBC)_2$ exhibited excellent chemical stability after soaking in a wide range of common organic solvents, including DMF, acetone, MeOH, H_2O and DCM (Figure S14). Thermogravimetric analysis (TGA) indicates a desolvation of $Cu_3(HFcHBC)_2$ initiated at ~100 °C and a noticeable weight loss started above 200 °C due to thermal decomposition (Figure S15). The porosity of $Cu_3(HFcHBC)_2$ was characterized by N_2 adsorption isotherms of the powders (collected film samples) at 77 K. The Brunauer-Emmett-Teller (BET) surface area was measured to be 426.9 $m^2 g^{-1}$ (Figure S16). The fitted pore size from the N_2 adsorption isotherm using non-local density functional theory (NLDFT) model was estimated to be 1.85 nm, which agrees well with the theoretical pore size (~1.80 nm).

To evaluate the crystal structure of $Cu_3(HFcHBC)_2$, we measured the powder X-ray diffraction (PXRD) for the collected film samples. The high crystallinity was confirmed by the sharp diffractions in the PXRD pattern. Prominent peaks at 2θ = 3.68°, 6.28° and 7.30° were assigned to the [100], [110] and [200] Bragg reflections, respectively (Figure 2b). To resolve the precise crystal structure, we isolated the rod-like $Cu_3(HFcHBC)_2$ single crystals from the film sample via sonication in ethanol and performed HRTEM and cRED studies.[40-41] The HRTEM image taken along [001] direction (Figure 2c) shows a highly ordered honeycomb lattice with $a = b$ = 27.8 Å. The corresponding fast Fourier transform (FFT) pattern shows good agreement with the honeycomb lattice (top inset, Figure 2c). Furthermore, the HRTEM image along the [110] direction reveals that the arrangement of the ligands is not parallel to a 2D plane but

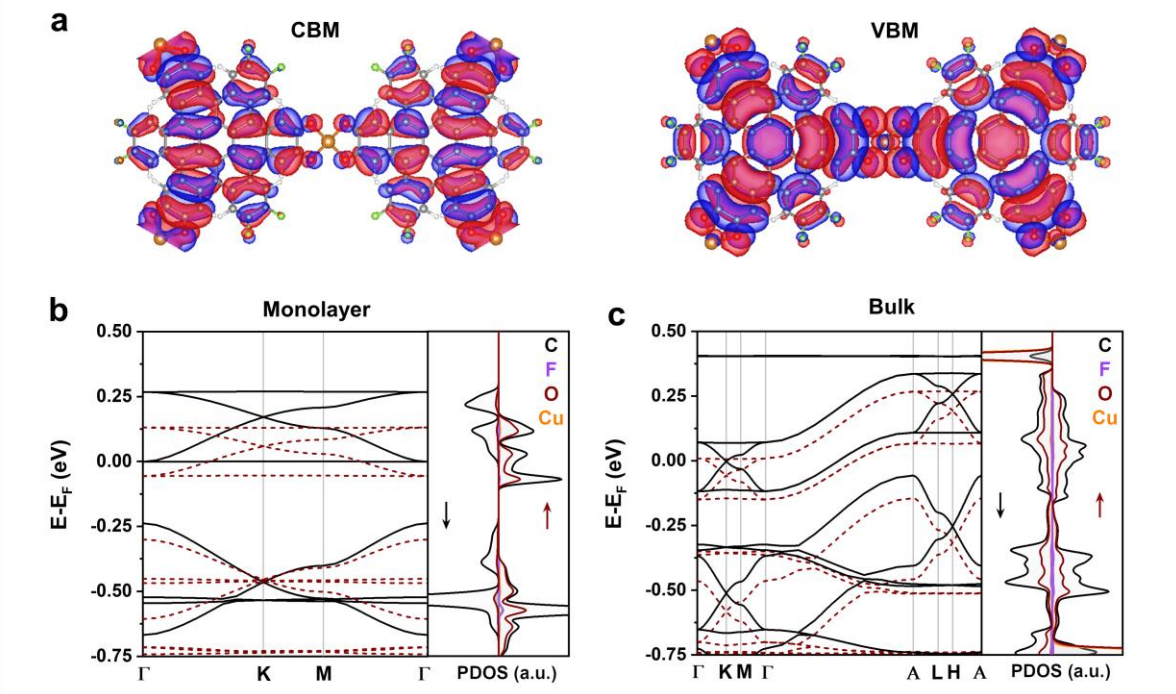

Figure 3. Electronic band structure of $Cu_3(HFcHBC)_2$. (a) the charge distribution at the conduction band minimum (CBM) and valence band maximum (VBM) of monolayer $Cu_3(HFcHBC)_2$. (b, c) Electronic band structure (spin up: red dashed line, spin down: black solid line) and projected density of states (PDOS) of monolayer (b) and bulk $Cu_3(HFcHBC)_2$ (c).

presents a wavy structure (Figure 2d). The distance between adjacent layers could be clearly measured as ~3.9 Å. Moreover, HRTEM images (Figure S18) and selected area electron diffraction (SAED) (Figure S19) patterns along [100] direction show a well-defined extended hexagonal channel throughout the crystal with d_{100} = 23.9 Å. The cRED method was applied to determine the precise crystal structure. cRED data has a resolution of 1.8 Å, from which the structure model was obtained using simulated annealing (Figures 2e and 2f, Figures S20 and S21). A square-planar CuO_4 unit was formed after linking the Cu^{2+} with two alternately arranged HFcHBC ligands (one with all -OH below the coronene plane and the other with all -OH above the coronene) (Figures 2g and 2h). The CuO_4 units surround each HFcHBC ligand to form an infinite 2D wavy layer with a honeycomb lattice ($a = b$ = 27.719(1) Å). The resulting $Cu_3(HFcHBC)_2$ crystal possessed an interlayer distance of c = 3.930(1) Å (Figure 2h) and a perfect AA stacking between the layers, which agree well with the HRTEM results. Pawley fitting was performed to refine the unit cell parameters of $Cu_3(HFcHBC)_2$. The unit cell parameters were refined as $a = b$ = 28.070(2) Å, c = 3.950(5) Å, and the R-values were converged to R_p = 0.0572, R_{wp} = 0.0865, and R_{exp} = 0.0587. (Table S3). To further validate the structure of $Cu_3(HFcHBC)_2$, the PXRD pattern was simulated by using the structural model obtained by cRED data and the refined unit cell parameters from Pawley fitting. The simulated PXRD pattern agrees well with the observed pattern (Figure S22). In view of all these evidences, $Cu_3(HFcHBC)_2$ was resolved to be a wavy 2D honeycomb structure, features an eclipsed the AA stacking model in the space group $P\bar{3}m1$.

Based on the established crystal structure with atom precision, the electronic band structure and projected density of states (PDOS) of $Cu_3(HFcHBC)_2$ were calculated using DFT calculations. The calculated surface charge distribution of the monolayer $Cu_3(HFcHBC)_2$ shows that π electrons are highly delocalized over the wavy 2D framework (Figure 3a). The electronic band structure features a Dirac cone at K points and two flat bands, with bands widely dispersed across the Fermi level, indicating an intrinsic metallic behavior (Figures 3b). The favorable alignment of the ligand and CuO_4 energy levels lowers the energy barrier for charge transport within the 2D plane. The AA eclipsed stacking structure also exhibits dispersed valence band and conduction band, with the latter crossing the Fermi level in both *Γ-K* and *Γ-A* directions with a broad band dispersion of about 0.2 eV (Figure 3c), supporting a metallic behavior. In $Cu_3(HFcHBC)_2$, the unique wavy structure enables to promote the formation of the ideal AA stacking structure, thereby enhancing the electronic coupling between the layers.[42-43] These results manifest a high degree of both in-plane and out-of-plane π-conjugation in $Cu_3(HFcHBC)_2$, promoting efficient charge transport.

The UV-vis-NIR spectrum of $Cu_3(HFcHBC)_2$ film shows broad absorption bands near the infrared region (around 1350 nm). The optical band gap was estimated to be ~0.71 eV from the onset of the near-infrared region and Tauc plots (Figure S25). We further probed the electron transport properties of $Cu_3(HFcHBC)_2$ via conductivity measurements. The $Cu_3(HFcHBC)_2$ thin films on Si/SiO_2 displayed an electrical conductivity of 0.037 S cm^{-1} at 300 K using van der Pauw methods (Figure 4a), which is almost two orders of magnitude higher than the MOF sample without F, indicating the benefits for introducing F substituents.[34] Variable-temperature conductivity measurements on macroscopic $Cu_3(HFcHBC)_2$ films revealed a thermally-activated charge transport behavior from 320 to 100 K. The activation energy E_a was derived from fitting the Arrhenius plot, which followed the $\sigma(T) = \sigma_0 \exp[-(E_a/k_BT)]$ (k_B is the Boltzmann constant). The fitted E_a of the measurement is

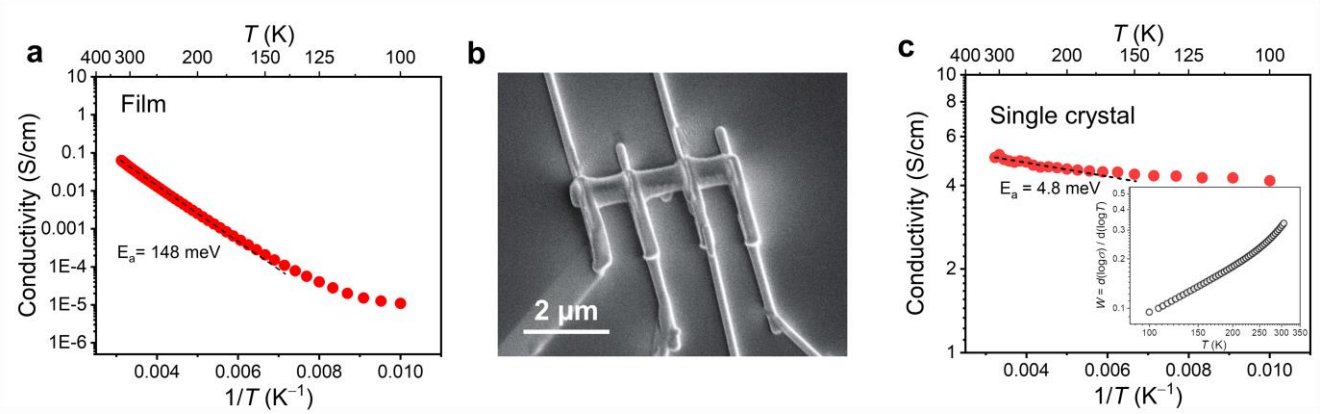

Figure 4. Charge transport properties of $Cu_3(HFcHBC)_2$ film and single crystal. (a) temperature-dependent conductivity of $Cu_3(HFcHBC)_2$ polycrystalline film (thickness, ~82 nm) ranging from 320 K to 100. (b) SEM of a single crystal $Cu_3(HFcHBC)_2$ device with Pt contacts. (c) temperature-dependent conductivity of $Cu_3(HFcHBC)_2$ single crystal ranging from 310 K to 100 K. Inset: Zabrodskii plots (double-logarithmic plot of $W = d(\log \sigma)/d(\log T)$ *vs.* T).

~148 meV. These results show an apparently semiconducting behavior for the film, in contrast to the metallic properties predicated by the calculation. Such behaviors is commonly observed in polycrystalline films or pellet samples for 2D c-MOF, in which the interparticle charge hoping across grain boundaries can dominate the transport behavior, making the intrinsic metallic nature hard to be observed.[44-46]

To reveal the intrinsic electronic properties of $Cu_3(HFcHBC)_2$, we performed electrical measurements on a single crystal. After isolating and transferring individual single crystals onto Si/SiO_2 substrates, focused ion beam (FIB) at ultrahigh vacuum was employed to construct Pt electrical contacts (Figure 4b and Figure S26) in a four-point probe measurement geometry. The electrical connection between the crystal and the Pt wires was confirmed to be Ohmic contact, as evidenced by the constant resistance (i.e. linear *I-V* characteristic) at different voltages (Figure S27). The single crystal device exhibits a conductivity of 5.2 S cm^{-1} after excluding the contact resistance at room temperature. The value is quite high compared to the previously reported c-MOF (Table S5) due to the strong π-orbital overlap between wavy 2D c-MOF layers. To gain insight into the possible influence of the absorbed water molecules on the electrical conductivity of $Cu_3(HFcHBC)_2$, we performed single crystal electrical transport measurements under air and vacuum conditions. As shown in Figure S28, the measured room-temperature conductivities of the samples are 4.25 S/cm and 5.2 S/cm under air and vacuum conditions, respectively. The small difference in the transport properties revealed no large influence from the possibly absorbed water molecules from air. Temperature-dependent measurement performed from 310 to 100 K presented a very weak thermally-activated transport behavior with an activation energy E_a of 4.8 meV (much lower than k_BT = 25.6 meV) evaluated by Arrhenius fitting at near room temperature, and it tended to be almost metallic at a lower temperature. To better understand the transport regime, Zabrodskii analysis is employed. A positive slope in a double-logarithmic plot of $W = d(\log \sigma)/d(\log T)$ against T which is observed in the single crystal device (Figure 4c) usually indicates the presence of intrinsic metallic states, while a negative slope which is observed in the polycrystalline film is a sign of insulating and hopping behavior.[45] Meanwhile, the conductivity of the single crystal does not decrease significantly (only by 20%) as the temperature drops, while that of the film decreases by four orders of magnitude from 310 to 100 K. Compared to the thin film composed of submicron-crystals, the single crystal exhibits two orders of magnitude higher room-temperature conductivities and 30 times lower activation energy. This indicates that grain boundaries are the major hindrance for charge transport in the polycrystalline films, which masks the metallic behavior inherent to the single crystal sample (Figure S29). The weakly thermally assisted charge transport in the single crystals could potentially be attributed to different factors: it is possible that stacking fault defects exist along the single-crystal wires on the length scale of several micrometers that is probed in the transport experiments. These could give rise to small energetic barriers. The weak temperature dependence may also reflect the temperature dependence of carrier scattering at impurities in the crystal or an electron-phonon coupling mechanism of the carriers. We cannot distinguish between these different mechanisms at this stage, but the weakly thermally assisted conductivity is consistent with a metallic transport regime. Ultraviolet photoemission valance band spectrum (UPS) measurement was further performed for the $Cu_3(HFcHBC)_2$ at 300 K (Figure S30). The result indicates that the Fermi level of $Cu_3(HFcHBC)_2$ cuts the valence band, supporting a metallic nature.[22]

As a proof-of-concept, we further evaluated the energy storage performance of $Cu_3(HFcHBC)_2$ as electrode materials in a three-electrode system using 5 M LiCl as aqueous electrolyte. As shown in Figure S31a, $Cu_3(HFcHBC)_2$ displays two pairs of redox peaks within the potential range of -0.6 to 0.8 V (vs Ag/AgCl), located at around -0.2 V to 0.3 V, respectively, suggesting a two-electron transfer process during the electrochemical charge/discharge process. In addition, Galvanostatic charge-discharge (GCD) curves of $Cu_3(HFcHBC)_2$ exhibit two obvious redox plateaus (Figure S31b). According to the GCD results, we determined that the maximum gravimetric capacitance of $Cu_3(HFcHBC)_2$ electrodes could reach 163.3 F g^{-1} at a current density of 0.5 A g^{-1} (Figure S31c), which shows potential applications in hybrid supercapacitors and aqueous lithium batteries.[47-49] Additionally, the $Cu_3(HFcHBC)_2$ also presents excellent long-term cycling stability. Even after 5000 cycles of charge/discharge process for at 5 A g^{-1}, the capacity retention of 2D c-MOF could still reach 97.31% with a high coulombic efficiency close to 100% (Figure S31d).

CONCLUSION

In conclusion, we have synthesized a novel Cu-catecholate wavy 2D c-MOF based on a non-planar HFcHBC ligand. Benefiting from the electronic deficient core and the contorted geometry of the HFcHBC, the resulting $Cu_3(HFcHBC)_2$ exhibits high crystallinity. As characterized by single crystal structure analysis utilizing cRED and HRTEM, $Cu_3(HFcHBC)_2$ presents an AA eclipsed wavy 2D honeycomb lattice, with the alternated arrangement of HFcHBC nodes linked by a square planar CuO_4 bond. Temperature-dependent conductivity measurement of the single crystal device demonstrates the metallic nature of $Cu_3(HFcHBC)_2$, with a room temperature conductivity of 5.2 S cm^{-1}. Our results could lead to a new generation of wavy 2D c-MOFs with metallic conductivity from the contorted ligand, we believe that the newly developed cHBC based c-MOF will provide new material platforms for electronic and energy applications. Moreover, the precise understanding of the structure-properties relationship of the

wavy 2D c-MOF can provide valuable inspiration and guidance for future 2D c-MOF design endeavors.

ASSOCIATED CONTENT

Supporting Information.
The Supporting Information is available free of charge via the Internet at http://pubs.acs.org.

Experimental methods, characterization data, NMR spectra, TEM images, XPS spectra, DFT calculations, and conductivity measurements.

AUTHOR INFORMATION

Corresponding Author

Zhiyong Wang- Center for Advancing Electronics Dresden (cfaed) and Faculty of Chemistry and Food Chemistry, Technische Universität Dresden, Dresden 01062, Germany; Max Planck Institute for Microstructure Physics, Weinberg 2, Halle (Saale) 06120, Germany; Email: wang.zhiyong@tu-dresden.de

Zhehao Huang- Department of Materials and Environmental Chemistry, Stockholm University, Stockholm SE-106 91, Sweden; Email: zhehao.huang@mmk.su.se

Henning Sirringhaus- Optoelectronics Group, Department of Physics, Cavendish Laboratory, University of Cambridge, Cambridge CB3 0HE, United Kingdom; Email: hs220@cam.ac.uk

Xinliang Feng-Center for Advancing Electronics Dresden (cfaed) and Faculty of Chemistry and Food Chemistry, Technische Universität Dresden, Dresden 01062, Germany; Max Planck Institute for Microstructure Physics, Weinberg 2, Halle (Saale) 06120, Germany; Email: xinliang.feng@tu-dresden.de

Renhao Dong-Center for Advancing Electronics Dresden (cfaed) and Faculty of Chemistry and Food Chemistry, Technische Universität Dresden, Dresden 01062, Germany; Key Laboratory of Colloid and Interface Chemistry of the Ministry of Education, School of Chemistry and Chemical Engineering, Shandong University, Jinan 250100, China; Email: renhao.dong@tu-dresden.de

Author

Jianjun Zhang - Center for Advancing Electronics Dresden(cfaed), Faculty of Chemistry and Food Chemistry, Technische Universität Dresden, Dresden 01062, Germany

Guojun Zhou – Department of Materials and Environmental Chemistry, Stockholm University, Stockholm SE-10691, Sweden

Hio-Ieng Un – Optoelectronics Group, Department of Physics, Cavendish Laboratory, University of Cambridge, Cambridge CB3 0HE, United Kingdom

Fulu Zheng - Bremen Center for Computational Materials Science, University of Bremen, Bremen 28359, Germany

Kamil Jastrzembski - Center for Advancing Electronics Dresden(cfaed), Faculty of Chemistry and Food Chemistry, Technische Universität Dresden, Dresden 01062, Germany

Mingchao Wang - Center for Advancing Electronics Dresden(cfaed), Faculty of Chemistry and Food Chemistry, Technische Universität Dresden, Dresden 01062, Germany

Quanquan Guo - Center for Advancing Electronics Dresden(cfaed), Faculty of Chemistry and Food Chemistry, Technische Universität Dresden, Dresden 01062, Germany

David Mücke - Central Facility for Electron Microscopy, Electron Microscopy of Materials Science Central, Facility for Electron Microscopy, Ulm University, Ulm 89081, Germany

Haoyuan Qi - Central Facility for Electron Microscopy, Electron Microscopy of Materials Science Central, Facility for Electron Microscopy, Ulm University, Ulm 89081, Germany

Yang Lu - Center for Advancing Electronics Dresden(cfaed), Faculty of Chemistry and Food Chemistry, Technische Universität Dresden, Dresden 01062, Germany; Max Planck Institute for Microstructure Physics, Weinberg 2, Halle (Saale) 06120, Germany

Yan Liang - Bremen Center for Computational Materials Science, University of Bremen, Bremen 28359, Germany

Markus Löffler - Dresden Center for Nanoanalysis (DCN), Center for Advancing Electronics Dresden (Cfaed), Technische Universität Dresden, Dresden 01069, Germany

Ute Kaiser - Central Facility for Electron Microscopy, Electron Microscopy of Materials Science Central, Facility for Electron Microscopy, Ulm University, Ulm 89081, Germany

Thomas Frauenheim - Constructor University, Campus Ring 1, Bremen 28759, Germany; Beijing Computational Science Research Center, Beijing 100193, China; Shenzhen JL Computational Science and Applied Research Institute, Shenzhen 518109, China

Aurelio Mateo-Alonso - POLYMAT, University of the Basque Country UPV/EHU, Avenida de Tolosa 72, 20018 Donostia-San Sebastian, Spain; Ikerbasque, Basque Foundation for Science, Bilbao 48011, Spain

Author Contributions

All authors have given approval to the final version of the manuscript. ‡These authors contributed equally.

Notes

The authors declare no competing financial interest.

ACKNOWLEDGMENT

The authors acknowledge cfaed and Dresden Center for Nanoanalysis (DCN) at TUD. This work is financially supported by ERC starting grant (FC2DMOF, No. 852909), EU Graphene Flagship (Core3, No. 881603), ERC Consolidator Grant (T2DCP), DFG projects (SFB-1415, No. 417590517; SPP 1928, COORNET), EMPIR-20FUN03-COMET, H2020-FETOPEN-

PROGENY (No. 899205) as well as the German Science Council and Center of Advancing Electronics Dresden (cfaed). H.U. and H.S. thank the Engineering and Physical Sciences Research Council (EPSRC) and the Japanese Society for the Promotion of Science (JSPS) for support through a core-to-core grant (EP/S030662/1). R.D. thanks Taishan Scholars Program of Shandong Province (tsqn201909047). A.M. thanks the support from the Basque Science Foundation for Science (Ikerbasque), POLYMAT, the University of the Basque Country, Diputación de Guipúzcoa, Gobierno Vasco (PIBA_2022_1_0031 and BERC programme) and Gobierno de España (Projects PID2021-124484OB-I00 and CEX2020-001067-M financed by MCIN/AEI/10.13039/501100011033) and Project (PCI2022-132921) funded by the Agencia Estatal de Investigación through the PCI 2022 and M-ERA.NET 2021 calls, technical and human support provided by SGIker of UPV/EHU and European funding (ERDF and ESF), funding from the European Research Council (ERC) under the European Union's Horizon 2020 research and innovation programme (Grant Agreement No. 722951), European Union under the Horizon Europe grant 101046231. Z.H. acknowledges the support by the Swedish Research Council Formas (2020-00831) and the Swedish Research Council (VR, 2022-02939). We thank Zichao Li and Shengqiang Zhou for Van der Pauw test, Dr. Jichao Zhang for EXAFS measurement, Xiaodong Li and Jiaxu Zhang for fruitful discussions.

REFERENCES

1. Wang, M.; Dong, R.; Feng, X., Two-dimensional conjugated metal–organic frameworks (2D c-MOFs): chemistry and function for MOFtronics. *Chem. Soc. Rev.* **2021,** *50* (4), 2764-2793.
2. Huang, X.; Zhang, S.; Liu, L.; Yu, L.; Chen, G.; Xu, W.; Zhu, D., Superconductivity in a Copper(II)-Based Coordination Polymer with Perfect Kagome Structure. *Angew. Chem. Int. Ed.* **2018,** *57* (1), 146-150.
3. Zhao, M.; Huang, Y.; Peng, Y.; Huang, Z.; Ma, Q.; Zhang, H., Two-dimensional metal-organic framework nanosheets: synthesis and applications. *Chem. Soc. Rev.* **2018,** *47* (16), 6267-6295.
4. Xie, L. S.; Skorupskii, G.; Dinca, M., Electrically Conductive Metal-Organic Frameworks. *Chem. Rev.* **2020,** *120* (16), 8536-8580.
5. Campbell, M. G.; Sheberla, D.; Liu, S. F.; Swager, T. M.; Dinca, M., Cu_3(hexaiminotriphenylene)$_2$: an electrically conductive 2D metal-organic framework for chemiresistive sensing. *Angew. Chem. Int. Ed.* **2015,** *54* (14), 4349-52.
6. Song, X.; Wang, X.; Li, Y.; Zheng, C.; Zhang, B.; Di, C. A.; Li, F.; Jin, C.; Mi, W.; Chen, L.; Hu, W., 2D Semiconducting Metal-Organic Framework Thin Films for Organic Spin Valves. *Angew. Chem. Int. Ed.* **2020,** *59* (3), 1118-1123.
7. Arora, H.; Dong, R.; Venanzi, T.; Zscharschuch, J.; Schneider, H.; Helm, M.; Feng, X.; Canovas, E.; Erbe, A., Demonstration of a Broadband Photodetector Based on a Two-Dimensional Metal-Organic Framework. *Adv. Mater.* **2020,** *32* (9), e1907063.
8. Sun, L.; Liao, B.; Sheberla, D.; Kraemer, D.; Zhou, J.; Stach, E. A.; Zakharov, D.; Stavila, V.; Talin, A. A.; Ge, Y.; Allendorf, M. D.; Chen, G.; Léonard, F.; Dincă, M., A Microporous and Naturally Nanostructured Thermoelectric Metal-Organic Framework with Ultralow Thermal Conductivity. *Joule* **2017,** *1* (1), 168-177.
9. Lu, Y.; Zhang, Y.; Yang, C. Y.; Revuelta, S.; Qi, H.; Huang, C.; Jin, W.; Li, Z.; Vega-Mayoral, V.; Liu, Y.; Huang, X.; Pohl, D.; Polozij, M.; Zhou, S.; Canovas, E.; Heine, T.; Fabiano, S.; Feng, X.; Dong, R., Precise tuning of interlayer electronic coupling in layered conductive metal-organic frameworks. *Nat. Commun.* **2022,** *13* (1), 7240.
10. Yu, M.; Dong, R.; Feng, X., Two-Dimensional Carbon-Rich Conjugated Frameworks for Electrochemical Energy Applications. *J. Am. Chem. Soc.* **2020,** *142* (30), 12903-12915.
11. Feng, D.; Lei, T.; Lukatskaya, M. R.; Park, J.; Huang, Z.; Lee, M.; Shaw, L.; Chen, S.; Yakovenko, A. A.; Kulkarni, A.; Xiao, J.; Fredrickson, K.; Tok, J. B.; Zou, X.; Cui, Y.; Bao, Z., Robust and conductive two-dimensional metal–organic frameworks with exceptionally high volumetric and areal capacitance. *Nat. Energy* **2018,** *3* (1), 30-36.
12. Hmadeh, M.; Lu, Z.; Liu, Z.; Gándara, F.; Furukawa, H.; Wan, S.; Augustyn, V.; Chang, R.; Liao, L.; Zhou, F., New porous crystals of extended metal-catecholates. *Chem. Mater.* **2012,** *24* (18), 3511-3513.
13. Sheberla, D.; Sun, L.; Blood-Forsythe, M. A.; Er, S. l.; Wade, C. R.; Brozek, C. K.; Aspuru-Guzik, A. n.; Dincă, M., High electrical conductivity in Ni_3 (2, 3, 6, 7, 10, 11-hexaiminotriphenylene)$_2$, a semiconducting metal–organic graphene analogue. *J. Am. Chem. Soc.* **2014,** *136* (25), 8859-8862.
14. Dong, R.; Han, P.; Arora, H.; Ballabio, M.; Karakus, M.; Zhang, Z.; Shekhar, C.; Adler, P.; Petkov, P. S.; Erbe, A.; Mannsfeld, S. C. B.; Felser, C.; Heine, T.; Bonn, M.; Feng, X.; Cánovas, E., High-mobility band-like charge transport in a semiconducting two-dimensional metal–organic framework. *Nat. Mater.* **2018,** *17* (11), 1027-1032.
15. Meng, Z.; Aykanat, A.; Mirica, K. A., Welding metallophthalocyanines into bimetallic molecular meshes for ultrasensitive, low-power chemiresistive detection of gases. *J. Am. Chem. Soc.* **2018,** *141* (5), 2046-2053.
16. Yang, C.; Dong, R.; Wang, M.; Petkov, P. S.; Zhang, Z.; Wang, M.; Han, P.; Ballabio, M.; Bräuninger, S. A.; Liao, Z., A semiconducting layered metal-organic framework magnet. *Nat. Commun.* **2019,** *10* (1), 1-9.
17. Yi, J. D.; Si, D. H.; Xie, R.; Yin, Q.; Zhang, M. D.; Wu, Q.; Chai, G. L.; Huang, Y. B.; Cao, R., Conductive Two-Dimensional Phthalocyanine-based Metal-Organic Framework Nanosheets for Efficient Electroreduction of CO2. *Angew. Chem. Int. Ed.* **2021,** *60* (31), 17108-17114.
18. Dong, R.; Zhang, Z.; Tranca, D. C.; Zhou, S.; Wang, M.; Adler, P.; Liao, Z.; Liu, F.; Sun, Y.; Shi, W., A coronene-based semiconducting two-dimensional metal-organic framework with ferromagnetic behavior. *Nat. Commun.* **2018,** *9* (1), 1-9.
19. Yao, M. S.; Lv, X. J.; Fu, Z. H.; Li, W. H.; Deng, W. H.; Wu, G. D.; Xu, G., Layer-by-Layer Assembled Conductive Metal-Organic Framework Nanofilms for Room-Temperature Chemiresistive Sensing. *Angew. Chem. Int. Ed.* **2017,** *56* (52), 16510-16514.
20. Huang, X.; Sheng, P.; Tu, Z.; Zhang, F.; Wang, J.; Geng, H.; Zou, Y.; Di, C.-a.; Yi, Y.; Sun, Y., A two-dimensional π–d conjugated coordination polymer with extremely high electrical conductivity and ambipolar transport behaviour. *Nat. Commun.* **2015,** *6* (1), 1-8.
21. Park, J.; Hinckley, A. C.; Huang, Z.; Feng, D.; Yakovenko, A. A.; Lee, M.; Chen, S.; Zou, X.; Bao, Z., Synthetic routes for a 2D semiconductive copper hexahydroxybenzene metal–organic framework. *J. Am. Chem. Soc.* **2018,** *140* (44), 14533-14537.
22. Dou, J. H.; Sun, L.; Ge, Y.; Li, W.; Hendon, C. H.; Li, J.; Gul, S.; Yano, J.; Stach, E. A.; Dinca, M., Signature of Metallic Behavior in the Metal-Organic Frameworks M_3(hexaiminobenzene)$_2$ (M = Ni, Cu). *J. Am. Chem. Soc.* **2017,** *139* (39), 13608-13611.
23. Stuparu, M. C., Corannulene: A curved polyarene building block for the construction of functional materials. *Acc. Chem. Res.* **2021,** *54* (13), 2858-2870.
24. Feng, C. N.; Kuo, M. Y.; Wu, Y. T., Synthesis, structural analysis, and properties of [8] circulenes. *Angew. Chem. Int. Ed.* **2013,** *125* (30), 7945-7948.
25. Amaya, T.; Hirao, T., A molecular bowl sumanene. *Chem. Commun.* **2011,** *47* (38), 10524-35.
26. Xiao, S.; Myers, M.; Miao, Q.; Sanaur, S.; Pang, K.; Steigerwald, M. L.; Nuckolls, C., Molecular wires from contorted aromatic compounds. *Angew. Chem. Int. Ed.* **2005,** *44* (45), 7390-7394.

27. Ball, M.; Zhong, Y.; Wu, Y.; Schenck, C.; Ng, F.; Steigerwald, M.; Xiao, S.; Nuckolls, C., Contorted polycyclic aromatics. *Acc. Chem. Res.* **2015,** *48* (2), 267-76.
28. Zbigniew R. Grabowski, a. K. R., Structural Changes Accompanying Intramolecular Electron Transfer: Focus on Twisted Intramolecular Charge-Transfer States and Structures. *Chem. Rev.* **2003,** *103*, 3899–4031.
29. Im, Y.; Kim, M.; Cho, Y. J.; Seo, J.-A.; Yook, K. S.; Lee, J. Y., Molecular Design Strategy of Organic Thermally Activated Delayed Fluorescence Emitters. *Chem. Mater.* **2017,** *29* (5), 1946-1963.
30. Mallia, A. R.; Salini, P. S.; Hariharan, M., Nonparallel Stacks of Donor and Acceptor Chromophores Evade Geminate Charge Recombination. *J. Am. Chem. Soc.* **2015,** *137* (50), 15604-7.
31. Martinez-Abadia, M.; Stoppiello, C. T.; Strutynski, K.; Lerma-Berlanga, B.; Marti-Gastaldo, C.; Saeki, A.; Melle-Franco, M.; Khlobystov, A. N.; Mateo-Alonso, A., A Wavy Two-Dimensional Covalent Organic Framework from Core-Twisted Polycyclic Aromatic Hydrocarbons. *J. Am. Chem. Soc.* **2019,** *141* (36), 14403-14410.
32. Martínez-Abadía, M.; Strutyński, K.; Lerma-Berlanga, B.; Stoppiello, C. T.; Khlobystov, A. N.; Martí-Gastaldo, C.; Saeki, A.; Melle-Franco, M.; Mateo-Alonso, A., π-Interpenetrated 3D Covalent Organic Frameworks from Distorted Polycyclic Aromatic Hydrocarbons. *Angew. Chem. Int. Ed.* **2021,** *60* (18), 9941-9946.
33. Martínez-Abadía, M.; Strutyński, K.; Stoppiello, C. T.; Lerma Berlanga, B.; Martí-Gastaldo, C.; Khlobystov, A. N.; Saeki, A.; Melle-Franco, M.; Mateo-Alonso, A., Understanding charge transport in wavy 2D covalent organic frameworks. *Nanoscale* **2021,** *13* (14), 6829-6833.
34. Xing, G.; Liu, J.; Zhou, Y.; Fu, S.; Zheng, J. J.; Su, X.; Gao, X.; Terasaki, O.; Bonn, M.; Wang, H. I.; Chen, L., Conjugated Nonplanar Copper-Catecholate Conductive Metal-Organic Frameworks via Contorted Hexabenzocoronene Ligands for Electrical Conduction. *J. Am. Chem. Soc.* **2023,** *145* (16), 8979-8987.
35. Hiszpanski, A. M.; Saathoff, J. D.; Shaw, L.; Wang, H.; Kraya, L.; Lüttich, F.; Brady, M. A.; Chabinyc, M. L.; Kahn, A.; Clancy, P., Halogenation of a nonplanar molecular semiconductor to tune energy levels and bandgaps for electron transport. *Chem. Mater.* **2015,** *27* (5), 1892-1900.
36. Dou, J.-H.; Arguilla, M. Q.; Luo, Y.; Li, J.; Zhang, W.; Sun, L.; Mancuso, J. L.; Yang, L.; Chen, T.; Parent, L. R., Atomically precise single-crystal structures of electrically conducting 2D metal–organic frameworks. *Nat. Mater.* **2021,** *20* (2), 222-228.
37. Zhang, Q.; Peng, H.; Zhang, G.; Lu, Q.; Chang, J.; Dong, Y.; Shi, X.; Wei, J., Facile bottom-up synthesis of coronene-based 3-fold symmetrical and highly substituted nanographenes from simple aromatics. *J. Am. Chem. Soc.* **2014,** *136* (13), 5057-64.
38. Dong, R.; Zhang, T.; Feng, X., Interface-assisted synthesis of 2D materials: trend and challenges. *Chem. Rev.* **2018,** *118* (13), 6189-6235.
39. Fan, K.; Zhang, C.; Chen, Y.; Wu, Y.; Wang, C., The chemical states of conjugated coordination polymers. *Chem* **2021,** *7* (5), 1224-1243.
40. Yang, T.; Willhammar, T.; Xu, H.; Zou, X.; Huang, Z., Single-crystal structure determination of nanosized metal-organic frameworks by three-dimensional electron diffraction. *Nat. Protoc.* **2022,** *17* (10), 2389-2413.
41. Huang, Z.; Grape, E. S.; Li, J.; Inge, A. K.; Zou, X., 3D electron diffraction as an important technique for structure elucidation of metal-organic frameworks and covalent organic frameworks. *Coord. Chem. Rev.* **2021,** *427*, 213583.
42. Kumar, R.; Aggarwal, H.; Srivastava, A., Of Twists and Curves: Electronics, Photophysics, and Upcoming Applications of Non-Planar Conjugated Organic Molecules. *Chemistry* **2020,** *26* (47), 10653-10675.
43. Jiang, D., Covalent Organic Frameworks: An Amazing Chemistry Platform for Designing Polymers. *Chem* **2020,** *6* (10), 2461-2483.
44. Debela, T. T.; Yang, M. C.; Hendon, C. H., Ligand-Mediated Hydrogenic Defects in Two-Dimensional Electrically Conductive Metal-Organic Frameworks. *J. Am. Chem. Soc.* **2023**, 145(20), 11387–11391.
45. Day, R. W.; Bediako, D. K.; Rezaee, M.; Parent, L. R.; Skorupskii, G.; Arguilla, M. Q.; Hendon, C. H.; Stassen, I.; Gianneschi, N. C.; Kim, P.; Dinca, M., Single Crystals of Electrically Conductive Two-Dimensional Metal-Organic Frameworks: Structural and Electrical Transport Properties. *ACS Cent. Sci.* **2019,** *5* (12), 1959-1964.
46. Skorupskii, G.; Le, K. N.; Cordova, D. L. M.; Yang, L.; Chen, T.; Hendon, C. H.; Arguilla, M. Q.; Dinca, M., Porous lanthanide metal-organic frameworks with metallic conductivity. *Proc. Natl. Acad. Sci. U S A* **2022,** *119* (34), e2205127119.
47. Sheberla, D.; Bachman, J. C.; Elias, J. S.; Sun, C. J.; Shao-Horn, Y.; Dinca, M., Conductive MOF electrodes for stable supercapacitors with high areal capacitance. *Nat. Mater.* **2017,** *16* (2), 220-224.
48. Zhou, S.; Kong, X.; Zheng, B.; Huo, F.; Stromme, M.; Xu, C., Cellulose Nanofiber @ Conductive Metal-Organic Frameworks for High-Performance Flexible Supercapacitors. *ACS Nano* **2019,** *13* (8), 9578-9586.
49. Li, W. H.; Ding, K.; Tian, H. R.; Yao, M. S.; Nath, B.; Deng, W. H.; Wang, Y.; Xu, G., Conductive metal – organic framework nanowire array electrodes for high - performance solid - state supercapacitors. *Adv. Funct. Mater.* **2017,** *27* (27), 1702067.

Table of Contents Graphic